Reliability Analysis of Crack Growth Occurrence for a Secondary Hull Component due to Vibration Excitation

Siri Kolle Kleivane[1]
Department of Marine Technology,
Norwegian University of Science and Technology,
Trondheim, Norway,
email: siri.k.kleivane@ntnu.no

Bernt J. Leira
Department of Marine Technology,
Norwegian University of Science and Technology,
Trondheim, Norway,
email: bernt.leira@ntnu.no

Sverre Steen
Department of Marine Technology,
Norwegian University of Science and Technology,
Trondheim, Norway,
email: sverre.steen@ntnu.no

Ship hull vibration is a significant contributor to fatigue crack growth and the major sources of vibrations are found to be the main engine vibration excitation, the wave-induced springing and whipping loads, and the action of the propeller. In the midship region, wave-induced loads and the main engine are the major contributors, whereas propeller excitation dominates in the aft region of the ship hull. No general method exists to solve all kinds of vibration problems and they need to be evaluated through a case-by-case approach. The complex and uncertain aspects of hull vibration and fatigue crack growth motivate the need for a reliability-based scheme for assessing the resulting fatigue crack propagation. In the present paper, a probabilistic formulation for the failure probability of the occurrence of crack propagation of a secondary hull component is outlined. A generic cargo hold model is analyzed with engine excitation and wave-induced loading as vibration sources, and a stochastic model for vibration response is outlined. The limit state is formulated as the possible occurrence of fatigue crack growth. The secondary hull component considered is a pipe stack support, which is a supporting component that attaches the cargo pipes to the wall inside a cargo tank. Different initial crack sizes are implemented to evaluate the adequacy of the applied stochastic model for vibration response and the accuracy of the estimated failure probability is assessed.

Keywords: Engine excitation, wave-induced loading, failure probability, FORM/SORM, Monte Carlo simulation, structural reliability analysis

1 Introduction

Ship vibration continues to be a major concern in the design, construction, and operation of vessels. Excessive vibration may lead to the malfunction of machinery and equipment or fatigue failure of local structural members. The main engine, the propeller and the hydrodynamic loading are identified as the main sources of vibration. Vibrations are observed at both global and local levels and constitute a complex vibration problem within the ship hull. Hydrodynamic loading is considered to result in both local and global wave-induced vibration, generally described as springing and whipping [1][2]. Wave-induced vibration, along with main engine vibration, is dominant in the amidship region, while the propeller excitation is predominantly located in the aft end of the vessel, especially in the hull area above the propellers. The focus of this work will be on vibration caused by engine excitation and wave-induced loading.

Springing and whipping result in nonlinear vertical bending moments acting along the ship hull girder. This loading can be simplified as the superposition of high-frequency and low-frequency load components, which due to the interaction between various frequencies and components gives rise to coupled damage effects [3][4]. The vertical wave-induced bending moment results from the change of distribution of the buoyancy forces along the ship length combined with hydrodynamic and internal forces associated with the wave-induced ship motions [5]. For this loading condition on the ship hull, springing and/or whipping can occur. Springing is generally defined as stationary resonance vibration due to waves with encounter frequencies coinciding with the natural frequency, typically for the vertical 2-node mode [6]. Whipping is a transient hull girder vibration caused by an impact and is the vibration phenomenon which may follow after slamming and this transient vibration can increase the vertical bending moment [2][6].

The two-stroke low-speed marine diesel engines have been favored as the prime mover for ocean-going vessels due to their high reliability and efficiency. However, these engines transfer their vibration directly onto the hull structure, because the engine is usually mounted directly onto the hull due to its large size and mass. The engine vibrations are generally categorized into external inertia forces and moments, resulting from the oscillating masses, and guide force couples, originating from the combustion process in the engine. The inertia moments have the potential to cause the largest vibration excitation in the ship hull and mitigation devices, such as moment compensators, are generally installed to counteract the critical orders of these external moments. With these external moments mitigated, the dominant modes of vibration for the engine are called the X-mode and H-mode, as seen in Fig. 1. The moments generated by these vibration modes are referred to as the guide force couples, where the X-mode causes a rocking of the engine block, and the H-mode moment causes a twisting of the engine block.

The main objective of this work is not focused on the advanced modelling of the vibration sources, such as developing a model of the whole ship structure including the engine, but rather on the consequences of vibration with regards to fatigue crack growth of a secondary component attached to the hull structure. In addition to the complexity of assessing ship hull vibration, fatigue crack growth is a very complex and uncertain phenomenon. Several parameters which describe the physics of the problem need to be considered and these are generally known only on an approximate level. Secondary structural components and equipment, such as supports for pipes and stringers, may be especially prone to crack growth if they are welded. Welded components are particularly susceptible to fatigue failure due to the welding procedure and the presence of the weld itself. The weld may be considered the

[1]Corresponding Author.

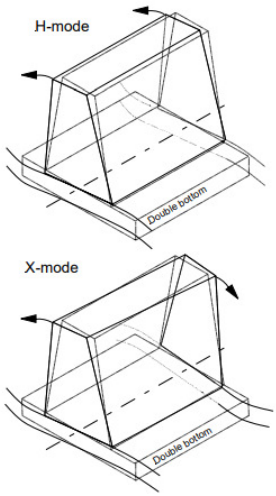

Fig. 1 Engine block H-mode and X-mode moments [7]

weakest part of a structure, and fatigue crack growth may initiate from items that are considered to be of minor importance for the ultimate load capacity of the structure [8]. The combined aspects of hull vibration and resulting fatigue crack growth motivate the need for a reliability-based scheme for assessing ship hull vibration and fatigue crack propagation of secondary details.

Fatigue is caused by dynamic loads and the calculation of relevant fatigue loading involves a global analysis of loads and their effect in terms of member forces, and a local analysis to determine their hot spot stresses [9]. Previous research on reliability with regards to vibration and fatigue crack growth has largely focused on only one of the major vibration sources and typically either considered it on a global scale or a local scale. Much research investigates the prediction of and the consequences of vertical wave-induced bending moment, and springing and whipping, on the ship hull girder reliability, such as presented by [2], [5], [10] and [11]. Extensive assessments concerning fatigue crack growth of ships and offshore structures are important aspects of the marine industry and are continuously under investigation and development. Moreover, an increasing number of studies also investigate the probabilistic and reliability aspects of fatigue crack growth occurrence, such as presented by [4], [12], [13] and [14]. However, there is a limited number of studies which looks at vibration response from several major vibration sources simultaneously and investigates the dependency between global and local vibration and its effect on secondary hull components or equipment. Such investigations are presented in this work to help improve the fatigue capacity of secondary details with the aim of the application of proper counteracting design measures.

To illustrate the possible lifetime of the secondary hull component, a simple event tree is presented in Fig. 2. Assuming an initial crack is present in the structure there will either be crack growth or no crack growth. If there is no crack growth the component can generally be considered safe from fatigue failure. For inspection and maintenance, there are many different schemes and methods which can be employed, but generally, if an inspection is done it will either detect damage or not. Moreover, there are typically several inspections done during the lifetime of a component, and there may or may not be conducted repairs. However, for all cases, the eventual outcome is either that the component fails (F) or is safe (S) from fatigue failure, as seen in Fig. 2. Note, even if repairs have been done the outcome may eventually still be a failure. In this work, we only investigate the probability of the branch for the occurrence of crack propagation but do not look further at the progression of crack growth. Moreover, any type of inspection and maintenance is not included in the model. The limit state formulation presented herein represents a conditional event of a propagating crack. This corresponds to the lifetime failure probability, and from this, the annual probability could then be computed as the probability increment per year as a function of time.

Table 1 Finite element model number of elements and nodes

Case	Elements	Nodes
Empty tanks	705740	1252199
25% filling level	729599	1331057
50% filling level	734445	1337396
75% filling level	732362	1330825
100% filling level	731348	1326467

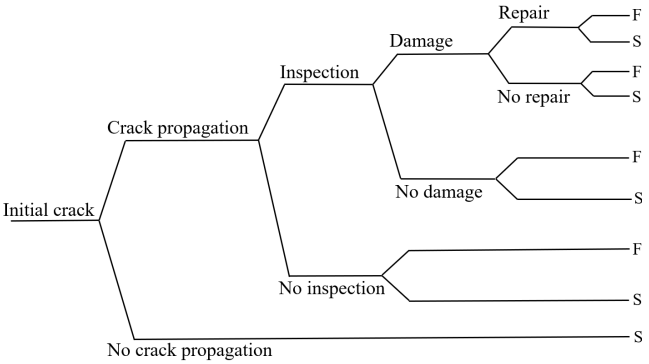

Fig. 2 Event tree for fatigue crack growth, F: fatigue failure, S: safe (no fatigue failure)

2 Finite Element Analysis of Vibration Response

2.1 Cargo hold model. A generic cargo hold finite element model has been developed consisting of ½ + 1 + ½ cargo hold units, divided by longitudinal bulkheads into transverse compartments as seen in Fig. 3. Different filling levels (full, partially loaded, and empty) are modelled, and an alternating load condition is implemented. This is assumed as a scenario where the wall to which the pipe stack support is connected experiences large forces due to the mass of the cargo and the applied loading. The modelling is based on solid elements and the welds are included in the model. The structural parts have element type SOLID187, and the cargo has element type FLUID220. For the cargo, only the mass of the fluid, that is the additional mass on the structure due to cargo in the tanks, is considered. Hydrodynamic aspects, such as free-surface dynamic motions are not accounted for at this stage and the free-surface is assumed to be stationary. The number of elements and nodes for each filling level case is given in Table 1. Boundary conditions are applied based on the guideline by DNV [15] for finite element analysis. The boundary conditions in the cargo hold analysis consist of rigid links applied at the model ends and a point constraint to restrict unwanted rotation of the model (see Table 3 in DNV-CG-0127 for further specification).

The component under investigation is the pipe stack support, as seen in Fig. 4. These components attach the cargo pump and its pipe stack to the tank wall. They are welded directly onto the tank wall during the installation of the pump at the shipyard. To investigate the vibration-induced stresses within the pipe stack supports, additional submodels are established, as seen in Fig. 5. One model consists of the whole pipe stack with its support connected to a cut-out section of the tank wall. Three smaller models of only cut-out sections of the supports are also developed. These models are essentially the same, but they are located at different parts of

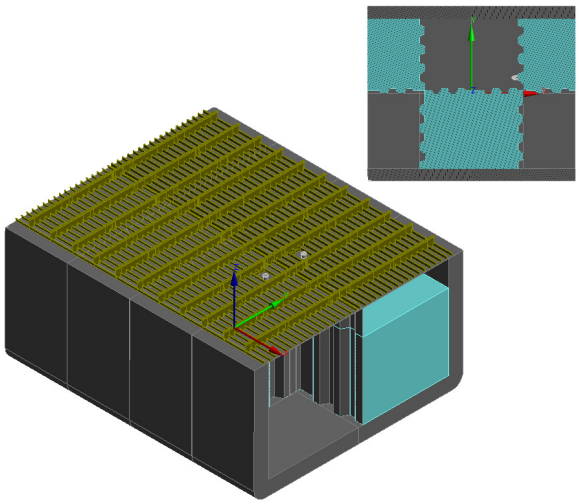

Fig. 3 Generic cargo hold model, here seen with alternating cargo configuration at 75% filling level

.

the global geometry, hence we are looking at all three supports to establish where the highest stresses occur. The submodels are analyzed using the sub-modelling technique where the boundary conditions are implemented as prescribed displacements. This is done by applying the nodal displacements of the global model to the corresponding boundary nodes on the local model, which allows us to examine the behavior around a specific, locally refined area without affecting the overall stiffness of the model. Consequently, the computational time will be smaller while the mesh can be refined on the local models.

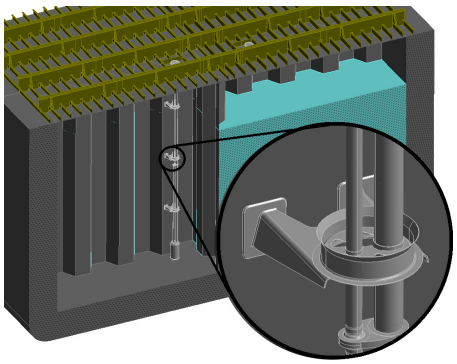

Fig. 4 Pipe stack support as the secondary hull component under consideration

2.2 Vibration analysis. The vibration analyses are conducted using Ansys Workbench with the application of the loading due to the engine excitation and the vertical wave-induced bending moment. These loading conditions are simulated separately; the cargo hold model is analyzed for different combinations of engine rpm and filling level in one analysis case, and the second analysis case is analyzed with the different filling levels and varying vertical bending moments. For the cases with no cargo in the tanks (empty tanks), the Harmonic Analysis module is adopted. For the cases with cargo in tanks, the Harmonic Acoustic module is adapted to take into account the mass effect of the cargo. A built-in application for the simulation of the sub-modelling cases is used for the local analyses of the pipe stack support. For further elaboration on the different modules and the sub-modelling application, reference is made to the Ansys Workbench User's Guide [16].

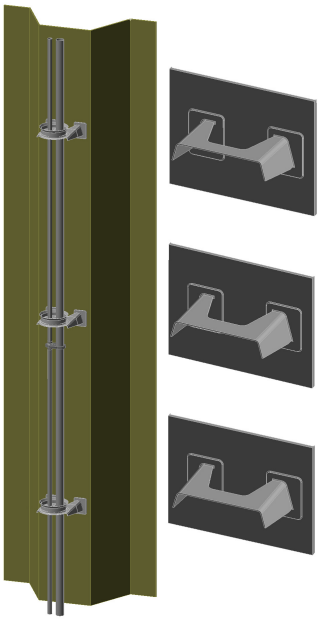

Fig. 5 Submodels of pipe stack (left) and pipe stack supports (right)

Stresses are evaluated as the response of interest since stress is in general considered to be the driving force for fatigue crack propagation. The type of stress evaluated is hot spot stress, which is obtained based on the recommended practice by DNV [17]. Since the modelling of the structure is based on solid elements with the welds included in the model, the effective hot spot stress is taken as the stress read out from a point located $0.5t$ away from the weld toe in the region where the maximum stress occurs, and t is the plate thickness at this location. DNV then gives the following formula to calculate the effective hot spot stress:

$$\Delta\sigma_{HS} = \begin{cases} 1.12\sqrt{\Delta\sigma_{\perp}^2 + 0.81\Delta\tau_{\parallel}^2} \\ 1.12\alpha|\Delta\sigma_1| \\ 1.12\alpha|\Delta\sigma_2| \end{cases} \tag{1}$$

The factor α depends on the welding class of the detail (see Table A-3 in DNV-RP-C203), which for the current detail can be taken as C2 with manual fillet weld, giving a factor α of 0.90. The stress components $\Delta\sigma_1$ and $\Delta\sigma_2$ are the principal stresses calculated by:

$$\Delta\sigma_{1,2} = \frac{\Delta\sigma_{\perp} + \Delta\sigma_{\parallel}}{2} \pm \frac{1}{2}\sqrt{(\Delta\sigma_{\perp} - \Delta\sigma_{\parallel})^2 + 4\Delta\tau_{\parallel}^2} \tag{2}$$

3 Probabilistic Formulation of Vibration Response

Three stochastic variables are established for the evaluation of vibration response: the engine speed (X) in rpm, the percentage filling level (Y) of cargo in the tanks, and the vertical wave-induced bending moment (Z). The vibration response due to engine excitation and wave-induce bending moment is evaluated and the influence of tank filling level is also analysed to establish the vibration response in the hold model. Based on the results, response functions for each variable are generated, where the stochastic variables will serve as input to these functions in the reliability assessment. The total stress response function is formulated as a combination of the individual response functions and is established based on a normalization procedure. This is done to obtain the correct units for the total response functions and to link the analysis cases together. Two main simulation cases are identified as described in Section 2.2, the first case consists of simulations with different

Table 2 Characteristics of the stochastic variables

Variable	Engine speed (rpm)	Filling level (%)	Wave moment (MNm)
Description	X	Y	Z
Distribution	Normal	Uniform	Weibull
Mean	86.1	50	52.2
Std	1.1	28.9	52.2
w	-	-	52.2
k	-	-	1
Upper-lower limits	80 - 90	0 - 100	1.5 - 105

*Std: standard deviation, w: scale parameter, k: shape parameter

Table 3 Engine external guide force couple moments

H-moment [kNm]			rpms		
Order	80	83	85	87	90
6	825.9	826.9	827.6	828.4	829.5
12	65.7	65.7	65.7	65.7	
X-moment [kNm]			rpms		
2	241.5	226.8	215.8	204.5	188.7
3	524.0	492.1	468.1	443.7	409.2
4	270.3	268.2	266.6	265.0	262.8
8	83.3	83.3	83.3	83.3	83.3
9	144.7	144.7	144.7	144.7	144.7
10	36.6	36.6	36.6	36.6	36.6

engine rpms and filling levels, and the second case consists of simulations with varying wave-induced VBMs and different filling levels. The response functions for the X- and Y-variable are based on the first analysis case and to find the total response for this case, the product of their normalized functions is applied. Subsequently, it is multiplied with their reference response values corresponding to a 50% filling level and 85rpm. The Z-function is established based on the second analysis case, and for this case, a constant 50% filling level is applied as the reference and the response function is normalized based on the median moment value. This normalized term is then added to the other term in the total response function. The resulting total stress response function is expressed as:

$$g_S(x,y,z) = g_{XYref}\left(g_{X,n}\left(\frac{x}{X_{ref}}\right)\cdot g_{Y,n}\left(\frac{y}{Y_{ref}}\right)\right)+g_{Zref}g_{Z,n}\left(\frac{z}{Z_{ref}}\right) \quad (3)$$

The total response function in Eq. (3) gives stress with a unit of MPa and has the three stochastic variables (X, Y, Z) as input variables in the reliability model. This stress response function gives the dependency of the total response to the local responses at the pipe stack support due to the combined effect of the different excitation sources (engine rpm and wave-induced VBM) and the filling level in the tank. The description of the three stochastic variables is further elaborated in the following sections.

3.1 Engine excitation. Modern engine manufacturing allows the manufacturer to analyze the engine performance already at the design stage, where excitation, structure and vibration response can be considered. The engine vibration is given as forces and moments emanating from the engine, caused by the combustion process in the engine and the motion of the reciprocating and rotating parts of the engine. These forces cause the engine block to deform and by this transmit vibrations into the engine foundation and subsequently into the hull. The magnitude of these forces and moments are specific for each engine since they depend on several factors, such as engine rating, the size of the engine and the number of cylinders. The engine manufacturers provide this data for their engines, and it is usually tabulated in the engine specifications. The data in the current work is provided for an engine typically used in medium-sized oil tankers, specifically a two-stroke low-speed 6-cylinder MAN B&W G50ME-C9.5 and the data are given for an engine rating of 6875 kW. Five different engine speeds (in rpm) are extracted and used in the vibration analysis. As described in Section 1, we are looking at guide force couples, and the specific moments for the different engine speeds used in the vibration analysis are given in Table 3.

The operational speed of the engine will influence the forces and moments generated by the engine. This is because these external forces and moments are influenced by the oscillating masses and the gas excitation processes in the engine, which change for different engine speeds. The engine speed as a stochastic variable is assumed to be normally distributed. This is based on research by [18], where a dataset of 16 crude oil tankers was investigated for estimation of the fuel consumption-speed curve for ships operating in ballast and loaded conditions. Moreover, the ship's speed in knots can be expected to be roughly linear with the shaft rpm [19]. By considering the speed interval for when the ship operating in the open sea and based on the assumption of linear relation, the speed is approximately normally distributed [18], as shown in Fig. 6 for engine speed ranging from 80 rpm to 90 rpm.

The statistical parameters of the distribution are given in Table 2. The soundness of assuming a normal distribution is evaluated

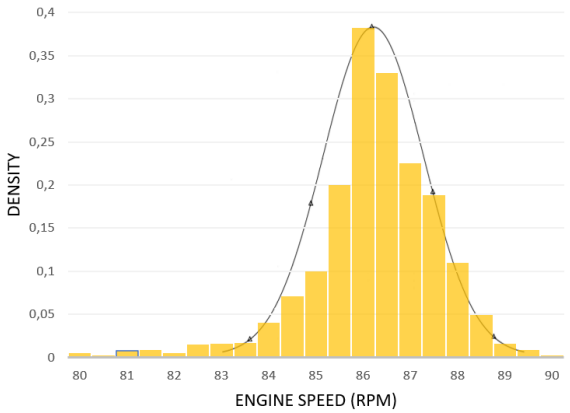

Fig. 6 Normally distributed engine rpm based on data given in [18]

by looking at the design point for failure probability calculation, and by fitting some alternative distribution to the data in Fig. 6 and comparing the estimated failure probabilities. Only negligible differences in the resulting probabilities were observed for these other cases.

The vibration analysis with engine speed excitation is done for combinations of five different rpms and five different filling levels in the tanks. The engine excitation is applied directly as moments scoped to a point mass which is a simplified representation of the engine, as seen in a) in Fig. 7. The point mass is scoped to the aft end of the model as a remote point with connection lines as seen in b) in Fig. 7. The magnitudes of the moments are established from the data provided by the engine manufacturer and implemented with their respective frequency of excitation. Five tank filling levels are applied in percentages which respectively correspond to the case of empty tanks (0%), 25%, 50%, 75% and fully loaded tanks (100%). The filling level as a stochastic variable is assumed to be uniformly distributed, with characteristics as given in Table 2.

3.2 Vertical wave-induced bending moment. Typically, the long-term cumulative probability distribution function of maxi-

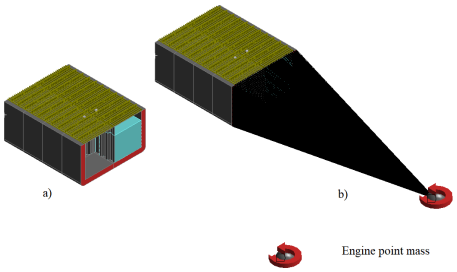

Fig. 7 a) Engine excitation applied as moment scoped to a point mass, b) Connection lines of remote point definition scoped to aft end of the model

mum vertical wave-induced bending moment is well described by a two-parameter Weibull distribution, this was shown by [20] and [5], among others. The vertical wave-induced bending moment as a stochastic variable is assumed to be Weibull distribution with shape parameter k and scale parameters w as defined by [5] and based on the linear prediction of the IACS-CSR formulation [21]. The distribution parameters are given in Table 2. The nonlinear effect of the vertical bending moment is not taken into consideration at this stage.

The vibration analyses are conducted for the five different filling levels and seven different moment magnitudes, including the median value for reference response. The applied moment values are obtained by discretization of the assumed Weibull distribution. The maximum hot spot stress at the support is obtained based on the procedure outlined in Section 2.2 and based on this a functional representation of the stress due to vertical wave-induced bending moment is obtained. Since no consideration of nonlinear effects is made and a linear formulation is applied, it may be expected (based on the load and the modelling simplifications) that there is a linear relationship between the stress response and the moment magnitude. For the full load, partial load, and ballast load conditions the Weibull equation remains the same and the loading imposed by the waves does not change.

4 Reliability Methods and Limit State Formulation

A significant amount of uncertainty is associated with fatigue crack growth and reliability methods are commonly applied in the theoretical and numerical investigation of fatigue. Structural reliability assessments are applied to establish failure probabilities of structural systems at any stage during their service life. The reliability assessment of ships and offshore structures generally involves multiple limit states and these are often correlated due to the complexity of such large systems. Therefore, simplifications are generally introduced to be able to analyze these systems. Simplifications are typically made in relation to the loading and response analysis, the strength characteristics and modelling, and how the different components and systems are connected. This introduces uncertainties in addition to the inherent uncertainties in the structural system.

The general reliability formulation (i.e., in terms of the probability of failure) can be expressed as:

$$p_f = P(G(\boldsymbol{x}) \leq 0) = \iint \ldots \iint_{G(\boldsymbol{x})\leq 0} f_{\boldsymbol{X}}(\boldsymbol{x})\, d\boldsymbol{x} \tag{4}$$

where $G(\boldsymbol{x}) \leq 0$ is referred to as the limit state function and the failure probability is defined as p_f. The joint probability density function is defined as $f_X(\boldsymbol{x})$, for the vector $\boldsymbol{x}$, which here will contain the three stochastic variables defined in Section 3. Moreover, the expression in Eq. (4) cannot usually be solved analytically and several different methods have been developed for solving this problem. Some extensively used methods are the Monte Carlo simulation methods and the FORM/SORM approximation methods.

4.1 Reliability calculation methods. The Monte Carlo simulation techniques generate a game of chance from known properties and involve simulating arbitrarily many experiments from random samples and observing the results to deduce the failure probability of the reliability problem. The general, most straightforward method may be called the crude Monte Carlo simulation or often just Monte Carlo simulation (MC). However, this method has a slow convergence of the estimated probability and to overcome this penalty, several different variance reduction techniques have been introduced creating a variety of different Monte Carlo simulation methods. A well-established method is the so-called importance sampling simulation, also sometimes called design point simulation (DSPS). This method is based on utilizing known information about the problem and constraining the simulation to the interesting regions. Consequently, fewer samples are needed to achieve the same level of accuracy as the general Monte Carlo simulation method.

The same principle applies to both methods, which is to interpret probability as a relative frequency [22], As part of Monte Carlo simulation, and an indicator function is applied which gives the value of 1 if failure occurs, and 0 if failure does not occur. The failure probability estimate is then calculated as:

$$\hat{p}_f = \frac{1}{N}\sum_{i=1}^{N} I\left(G(\hat{\boldsymbol{x}}_i)\right) = \frac{k}{N} \tag{5}$$

where $G(\boldsymbol{x})$ is the limit state function, I is the indicator function, k is the number of failure events and N is the total number of sample values in the simulation. For the importance sampling method, a modified expression for the failure probability estimate is formulated by introducing an importance-sampling probability density function (pdf), $h(\boldsymbol{x})$, which is intended to represent the region of most interest. The probability estimate for the importance sampling method is then expressed as:

$$\hat{p}_f = \frac{1}{N}\sum_{i=1}^{N} I\left(G(\hat{\boldsymbol{x}}_i)\right) \frac{f_X(\hat{\boldsymbol{x}}_i)}{h(\hat{\boldsymbol{x}}_i)} \tag{6}$$

The region for the importance sampling pdf may be difficult to identify and a general procedure is to use the computed design point in order to identify the region of interest [23]. Asymptotic approximation techniques or optimization techniques are typically used to establish the design point. Such a method can be the first-order reliability method (FORM), and in connection with simulation based on the design point, a FORM analysis is first performed to identify the design point. The importance sampling simulation is subsequently performed based on application of a sampling density which is centered at the design point.

The first-order reliability method (FORM) and the second-order reliability method (SORM) are asymptotic methods which approximate the integral in Eq. (4) by transforming the problem from the given variable space, say $\mathbf{x}$, to the standard normal space, say $\mathbf{u}$ [24] [25]. This transformation is generally performed by application of the Rosenblatt transformation, which preserves the statistical properties of the model during the mapping from the input variable space to the standard normal space [26].]. In general, this transformation needs to be done numerically, but the principle is illustrated for a single variable in Fig. 8. After the transformation of variables, the methods approximate the boundary surface of the so-called "safe domain" by a first order (FORM) or second order (SORM) shape. The integration from Eq. (4) is then conducted based on the approximated surface.

The general-purpose probabilistic calculation tool Proban is utilised for reliability calculations. A variety of failure probability approximation and simulation methods are contained in this program, which makes it suitable for structural reliability analysis calculations. For further elaboration on how the different reliability calculation methods are implemented in the program, reference

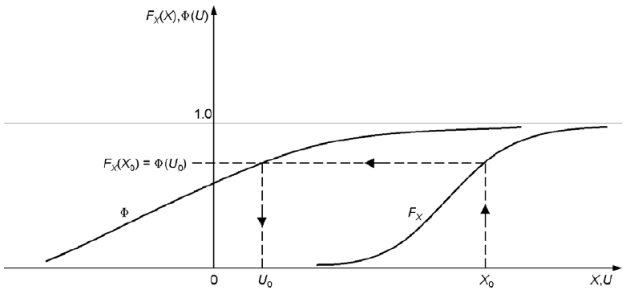

Fig. 8 Rosenblatt transformation for a single variable [27]

is made to the theory and user manuals [27][28]. Proban is a command scripted program, and the developed reliability model is implemented as a script in the program, and the above-mentioned reliability methods (MC, DSPS, FORM and SORM) are subsequently assigned for estimating the probability of failure.

4.2 Limit state for fatigue crack growth. Fatigue is caused by cyclic loads and in many cases these loads may give stresses less than yield stress, where damage per cycle may be quite insignificant and may not even be detectable. However, over a load history for which the ship may run into cycles in the order of 10^8, the accumulated fatigue damage may affect the integrity of the structure [29]. Thus, the calculation of fatigue loading and damage involves estimating stress ranges in various sea states and operational conditions in the long-term period. The two-parameter Weibull distributions have generally been used to quantify the probabilistic characteristics of fatigue damage and life [30]. In the current research, we only look at the possible occurrence of crack growth, assuming a crack is already present in the structure, which is generally assumed for welded structures [29]. Thus, the crack initiation stage is neglected, and the investigations herein concern whether the crack will start to grow when exposed to the different loading scenarios considered. It is to be noted that linear elastic fracture mechanics (LEFM) is assumed for the current investigations. However, the initial size of cracks in welded structures is generally short, and the applicability of LEFM may be discussed, as opposed to elastic-plastic fracture mechanics (EPFM) which is the fracture mechanics theory concerned with very short cracks.

Reliability assessments are typically based on the likelihood of limit state violation. A limit state is considered to be a condition beyond which the structure or system does not fulfil its specified design criteria. The limit state formulation as defined in Eq. (4) gives the regions of the parameter space which correspond to safe or unsafe conditions. The limit state presently is formulated as the occurrence of crack propagation, assuming that a surface crack is already present in the pipe stack support. A typical assumption for a three-dimensional surface crack is a semi-elliptical shape. The occurrence of crack propagation is based on the formulation of a maximum allowable stress before such a propagation occurs. This can be considered as a stress limit for which there is no fatigue damage if stresses are below this limit stress value, meaning that a crack will not grow. However, it is to be noted that cracks may propagate at stresses below this established limiting stress, as ships in service are exposed to variable stress histories. This aspect is not taken into consideration at this stage.

In the current investigations, the maximum allowable stress before crack propagation occurs is established based on empirical formulations for stress intensity factor (SIF) calculations [31] and a threshold value for crack growth [32]. The stress limit is formulated as follows:

$$S_{limit} = \frac{\Delta K_0}{\sqrt{\pi \frac{a_i}{Q}} \cdot F} \tag{7}$$

$$Q = 1 + 1.464\left(\frac{a_i}{c_i}\right)^{1.64} \tag{8}$$

where Q describes the approximate shape function of an ellipse and a and c are the crack size in depth and surface direction, respectively. The parameter F is called the geometry function and is dependent on the initial crack size, the geometry of the crack and the configuration of the loading. Assuming the initial crack size is known, the value of F can be estimated by using the graphs developed by [31], as given in Fig. 9. This figure shows typical results from the stress-intensity factor equation given in Eq. (7) for a semi-elliptical surface crack in a plate under bending loading.

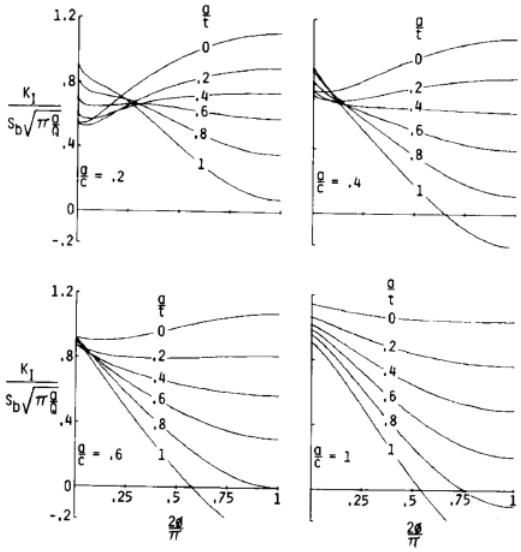

Fig. 9 Results from SIF equation according to [31]

The parameter ΔK_0 is a threshold stress intensity factor defined here as a fatigue crack growth threshold. Recommended values for ΔK_0 are typically given in different standards, and their value will vary depending on different factors, such as environment (air or corrosive) and type of metal (authentic, ferrous, etc. for steel). British Standard gives a guide to methods for assessing the acceptability of flaws in metallic structures (BS7910) and they provide different data required for assessment. In their standard BS7910, they give a guideline for the assessment of fatigue (see Section 8 in [32]). For welded steel joints they recommend a fatigue crack growth threshold value of ΔK_0 = 63MPa (see Section 8.2.3.6, Table 6 in [32]). The assessment of fatigue crack growth in this standard is based on fracture mechanics using Paris law:

$$\frac{da}{dN} = C(\Delta K)^m = C(\Delta S\sqrt{\pi a}F)^m \tag{9}$$

and for which they state that if $\Delta K < \Delta K_0$ the crack growth rate is assumed to be zero. The limit state function corresponding to the occurrence of a propagating fatigue crack is then formulated as:

$$G(x) = S_{limit} - f_S \leq 0 \tag{10}$$

where f_S is the total stress response function at the pipe stack support as given in Eq. (3).

The initial crack size in welded structures is very difficult to establish and different estimates are found in the literature (e.g., [32][33]). In the current formulation of the limit state, the form function and the maximum allowable stress are dependent on the initial crack size. Hence, to evaluate the effect that it has on the estimated failure probabilities, different values for initial crack size are investigated. This is presented in Table 4 where the maximum

Table 4 Maximum allowable stress for different initial crack sizes

Analysis case	Initial size [mm] a_i	c_i	F[-]	S_{limit}[MPa]
1	0.1	0.3	1.0	125
2	0.2	0.5	1.0	91
3	0.3	0.5	1.0	82
4	0.4	0.8	1.0	68
5	0.5	1.0	1.0	60
6	0.6	1.0	0.95	61

allowable stresses for the different cases have been calculated based on Eq. (7).

To evaluate the significance of the estimated failure probabilities, criteria for acceptability need to be defined. However, establishing an exact criterion for the acceptable probability of failure is challenging as it needs to be based on different aspects and parameters which are generally only known on an approximate level. This might be based on experimental investigation and operational experience. Moreover, for the investigations presented here, no such information is available but a probability of failure between 1 – 5 % is considered as not being critical for the pipe stack support.

5 Resulting vibration response at pipe stack support

The cargo hold model is analysed for each simulation case as described earlier with the combination of different excitation sources and filling levels. A sub-modelling technique in Ansys Workbench is utilised to analyse the cut-out section of the pipe stack and supports to identify the critical support. The critical support is the support that experiences the largest stresses, and for most of the simulation cases, this is identified as the bottom support. When this critical support is identified, the submodel of the support component is investigated further for hot spot stress calculations using the formulas presented in Eqs. (7) and (8). An example of a hot spot at the pipe stack support is presented in Fig. 10.

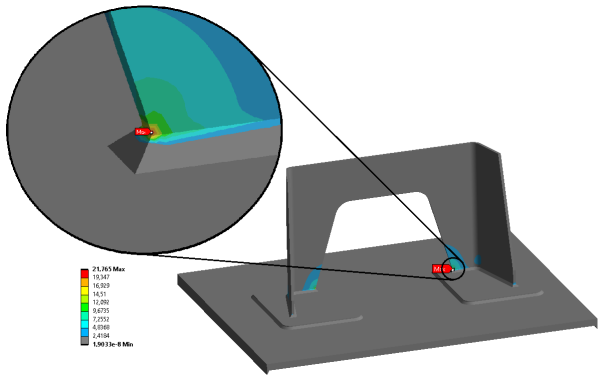

Fig. 10 Example of a hot spot at pipe stack support

Two data sets of stress response values are obtained, one for each of the two main simulation cases. Further, the response values are averaged for their respective excitation source which gives five data points of stress response values for engine excitation, and seven data points are obtained for wave-induced VBM excitation. The filling level is averaged based on the first simulation case, and five data points for stress response depending on the filling level are also established. These data points are used in the curve fitting procedure to establish the individual response stress functions for each of the variables. The data points for the different filling levels and the engine speed are presented in Table 5, with engine speed denoted RPM and filling level denoted FL. The data points for the wave-induced VBM are presented in Table 6.

Table 5 Stress data points for engine speed and filling level

RPM	Stress [MPa]	FL [%]	Stress [MPa]
80	3.447	0	0.201
83	2.978	25	0.509
85	4.239	50	1.645
87	5.518	75	8.830
90	8.349	100	13.346

Table 6 Stress data points for wave-induced VBM

VBN [MNm]	Stress [MPa]
1.5	0.053
13.0	0.459
36.0	1.271
53.3	1.882
59.0	2.083
82.0	2.895
105.0	3.707

6 Resulting Reliability Model and Probability Estimation

6.1 Stochastic model of vibration response. To establish the total response function given in Eq. (3), the individual response function for each variable (X, Y, Z) is established based on a curve fitting procedure using MATLAB. The data points for the stress values from the vibration analysis given in Section 5 for each variable are plotted against built-in functions in MATLAB and a best-fit approach is applied based on goodness of fit statistics. Three statistical parameters are evaluated, (i) the sum of squares due to error (SSE) which should have a value as close to zero as possible, (ii) the R-square which should have a value as close to one as possible, (iii) and the root mean squared error (RMSE) which should be as close to zero as possible. The resulting goodness of fit for the established response functions is given in Table 7.

The engine speed variable X is fitted by means of harmonic functions as shown in Fig. 11, based on the data given in Table 5. The corresponding normalized response function is given in Eq. (11).

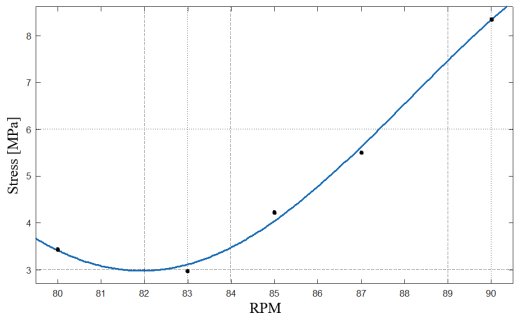

Fig. 11 Engine speed response curve

$$g_{X,n}(x) = 1.56 + 0.42\cos(21.71x) - 0.75\sin(21.71x) \quad (11)$$

The stress response corresponding to the filling level variable Y is fitted to a Gaussian equation as plotted in Fig. 12, based on the data given in Table 5. The corresponding normalized response function is given in Eq. (12).

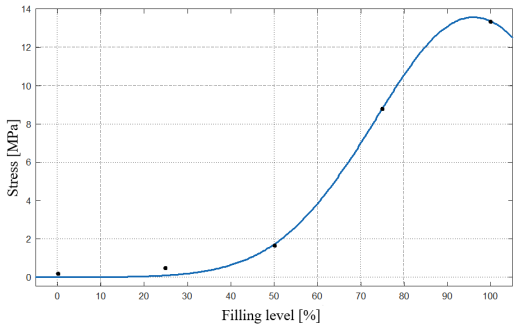

Fig. 12 Filling level response curve

Table 7 Goodness of fit statistics

Variable	SSE [MPa^2]	R-square [-]	RMSE [MPa]
X	0.071	0.996	0.266
Y	0.214	0.999	0.327
Z	0.0	1.0	0.0

$$g_{Y,n}(y) = 8.25 \cdot e^{-(\frac{y-1.92}{0.64})^2} \tag{12}$$

From Fig. 12 it is seen that the maximum stress value is at a point lower than 100% filling level. To evaluate the appropriateness of this, different functional representation was investigated and it was verified that the calculated failure probabilities are not sensitive to the detailed shape of the interpolation functions for the filling level response. For example, representing the filling level stress response by a sum of sines function resulted in a 1% difference in the failure probabilities, compared to the applied Gaussian function.

The stress response due to the moment variable Z is fitted to a linear equation as plotted in Fig. 13 based on the data given in Table 6, with the corresponding normalized response function given in Eq. (13).

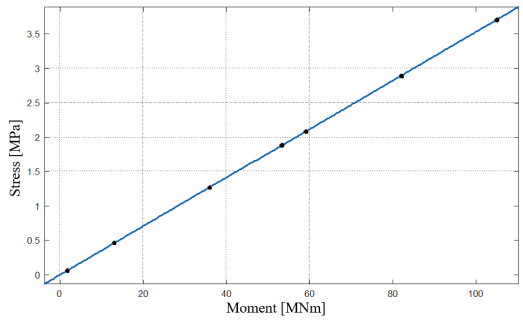

Fig. 13 Bending moment response curve

$$g_{Z,n}(z) = 1.0 \cdot z \tag{13}$$

From Table 7 it is seen that the goodness of fit for the Z variable is satisfactory, as can be assumed for a linear fit. For the X and Y variables, the SSE and R-square are satisfactory. This means there is only a minor deviation of the response values from the fit to the response values from the data, and the fit is successful in explaining the variation of the data. The RMSE, however, is sufficient for the X and Y variables, but there is a possibility of improvement.

Table 8 Estimated failure probabilities

Analysis cases	Failure probabilities [%] MC	DSPS	FORM	SORM
1	0	0	0	0
2	0.014	0.016	0.036	0.014
3	0.168	0.162	0.346	0.143
4	2.088	2.100	3.836	1.954
5	5.073	5.197	8.235	5.207
6	5.803	5.706	8.981	6.000

*MC: Monte Carlo simulation
*DSPS: Design point simulation (importance sampling)

Table 9 Importance factors of excitation sources

Variable	X	Y	Z
Importance factor	49.8	47.9	2.3

An unsafe limit state condition is reached when the resulting stress from this combined response function exceeds the maximum allowable stress established by Eq. (7), as formulated in Eq. (10). The combined response function is based on the assumption of statistical independence. This is to some extent reasonable for the X and Y variables since the ship's speed is generally determined based on the voyage together with environmental conditions and is not related to the amount of cargo being transferred. However, the Z variable may be correlated to both the X and Y variables, since the magnitude of the moment is dependent on buoyancy forces, and hydrodynamic and internal forces associated with the wave-induced ship motions, for which all are dependent on the ship's speed and mass of the vessel (which is affected by the cargo).

The data points for vibration response based on the five different values for engine speed and filling level, and the seven values for wave-induced VBM, are relatively small sets of data points. However, due to the computational demand for each simulation case, a trade-off between the simulation time and the number of data points simulated was conducted to reduce the computational time. Moreover, for the wave-induced vertical bending moment, nonlinear effects have not been considered. These simplifications represent limitations in the adequacy and accuracy of the developed stochastic model.

6.2 Failure probabilities. The developed reliability model is implemented into Proban as a script, where the defined stochastic variables are assigned to their distributions using their characteristics as defined in Table 2. The response functions in Eqs. (11)-(13) are defined and the respective stochastic variables are assigned to these functions. Then the total response function in Eq. (3) is defined. Further, the limit state formulation given in Eq. (10) is implemented to define the basic event and the different reliability methods outlined in Section 4.1 are subsequently assigned for the failure probability calculations.

The estimated failure probabilities are presented in Table 8 for the different analysis cases given in Table 4. The Monte Carlo simulation is run with 500 000 samples and for the importance sampling simulation (DSPS), 100 000 samples were used. Proban is very fast in its calculations and these sample sizes run in a matter of seconds. Based on a sensitivity analysis of sample size, the applied sample sizes are deemed sufficient to obtain stable results in the probability calculations. To look at the dependency of the stochastic variables on the results, the importance factors are presented in Table 9 as averaged values over the different cases. Importance factors indicate the importance of modelling the stochastic variables as distributions rather than as fixed-value variables [27].

The soundness of the assumption of a normal distribution for the engine speed presented in Fig. 6 was evaluated by investigating the

design point and applying other distributions for comparison. The design point, also referred to as the linearization point for calculations in Proban, is the point of maximum likelihood on the event boundary. Cases 1-3 in Table 4, giving the larger failure probabilities in Table 8, have design points around 88-89 rpm, while cases 4-6 in Table 4, giving the smaller failure probabilities in Table 8, have design points around 86-87 rpm. The normal distribution has its best fit in this region, as seen in Fig. 6, meaning that the important part of the data is adequately decided by the distribution. Moreover, the overall results of the failure probabilities, presented in Table 8, are not significantly influenced by representing engine speed with other probability distributions.

The results in Table 8 are plotted against the maximum allowable stress, as presented in Fig. 14. Based on Eq. (7) it is seen that for an increasing initial crack size, the maximum allowable stress before crack propagation occurs will decrease. In Fig. 14 it is seen that as the maximum allowable stress decreases the probability of failure increases. A smaller maximum allowable stress value means a larger initial crack size, as seen from Eq. (7). This means that for a larger initial crack size (smaller maximum allowable stress) there is a larger probability that the crack will start to grow under the current investigations. The plot presented in Fig. 14 may help to evaluate if a crack will start to grow or not for a set of given conditions. Moreover, the result from the Monte Carlo simulation and the importance sampling simulation (DSPS) coincide with those of the SORM approximation, while the FORM approximation deviates from the others. This may indicate that the failure surface is of second order or higher, displaying nonlinear characteristics. Therefore, the approximations by FORM may not be as accurate as the other estimates. The similarity in failure probability estimation from MC, DSPS and SORM methods provided support for the integrity of the obtained values. However, these results have not been compared with experimental or measured data. The accuracy of the results is only compared between the applied numerical methods, which must be kept in mind when discussing the credibility of the estimated failure probabilities.

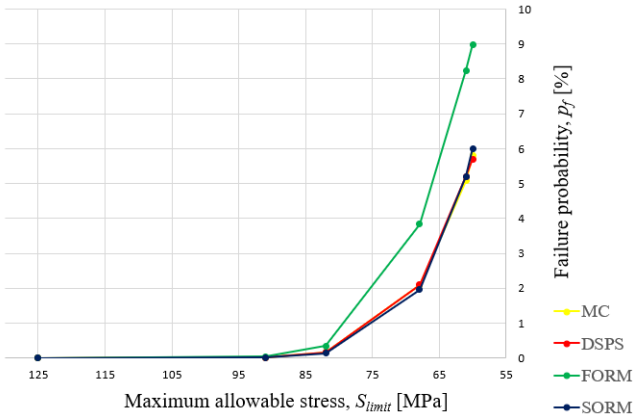

Fig. 14 Probability of failure plotted against maximum allowable stress

Looking at the importance of the different excitation sources presented in Table 9 it is seen that the wave-induced vertical bending moment has a minor effect compared to the engine excitation. The filling level and engine excitation have a significant influence on the vibration-induced stress response and they are seen to have almost equal importance to the response.

Evaluating the failure probabilities concerning the specified criterion for acceptable probability, the applied loading of engine excitation and wave-induced loading implies that cracks may start to grow for an initial crack size larger than 0.5mm in depth direction. However, it is to be noted that such acceptance criteria are very difficult to establish. This is one of the drawbacks of probability assessment. Based on the available information and provided data in this work, it can only be concluded that the evaluated problem has failure probabilities which may indicate that cracks can start to grow under these current conditions. Furthermore, the occurrence of crack growth has only been evaluated for a random point in time. The next step for further development of the framework herein may then be to evaluate loading over time to investigate the progression of a propagating crack and investigate the time it takes for an initial crack to grow to a critical size, which can be considered as representing fatigue failure of the secondary component.

7 Conclusions

This paper presents the development of a reliability model for failure probability estimation of the possible occurrence of crack growth of a pipe stack support connected to the inside of the cargo tank wall. Vibration responded due to main engine excitation and wave-induced loading is simulated using FEA. Three stochastic variables are defined and vibration response functions are developed for each variable. The functional representations of the stochastic variables are sufficiently satisfactory regarding the evaluation of their statistical parameters.

The probability of failure with regard to the possible occurrence of crack growth is investigated using different reliability methods and for different initial crack sizes of the welds in the pipe stack supports. The estimated failure probabilities imply that crack propagation may occur under the current conditions defined in this study and further investigation of the progression of crack growth and time until failure can be conducted by further developing the resulting reliability model presented in this work. This corresponds to looking at the branch of the event tree presented in Fig. 2, which represents the event that crack growth occurs and then evaluating the probability that a propagating crack will reach a critical level, or when it will reach a critical value. This may be conducted by looking at long-term responses to different sea states and operational conditions.

It is believed that further development of the reliability model for the support component presented herein may help to establish a framework and a computational tool to improve the fatigue capacity of such components.

Nomenclature

$\Delta\sigma_{hs}$ = hot spot stress range [MPa]
$\Delta\sigma_{\perp}$ = stress range component perpendicular to weld toe [MPa]
$\Delta\sigma_{\parallel}$ = stress range component parallel to weld toe [MPa]
α = welding class factor [-]
$\Delta\sigma_1$ = first principal stress [MPa]
$\Delta\sigma_2$ = second principal stress [MPa]
$\Delta\tau_{\parallel}$ = shear stress parallel to the weld toe [MPa]
Std = Standard deviation
w = scale parameter in Weibull distribution [MNm]
k = shape parameter in Weibull distribution [-]
p_f = failure probability
$G(x)$ = limit state function
$f_S(x)$ = total stress response joint probability density function
S_{limit} = maximum allowable stress [MPa]
ΔK_0 = fatigue crack growth threshold stress intensity factor range [MPa$\sqrt{\text{mm}}$]
a_i = initial crack size in depth direction [mm]
c_i = initial crack size in surface direction [mm]
F = geometry function [-]
Q = shape function for an ellipse [-]
g_{ref} = refernece stress response [MPa]
g_1 = engine speed response function [MPa]
$g_{1,n}$ = normalized engine speed response function [-]
g_2 = filling level response function [MPa]
$g_{2,n}$ = normalized filling level response function [-]
g_3 = wave moment response function [MPa]
$g_{3,n}$ = normalized wave moment response function [-]
MC = Monte Carlo simulation

DSPS = Design point simulation (importance sampling)
FORM = First order reliability method
SORM = Second order reliability method
SSE = the sum of squares due to error
RMSE = root mean squared error

References

[1] Storhaug, G., 2014, "The measured contribution of whipping and springing on the fatigue and extreme loading of container vessels," International Journal of Naval Architecture and Ocean Engineering, **6**(4), pp. 1096–1110.

[2] Pal, S. K., Ono, T., Takami, T., Tatsumi, A., and Iijima, K., 2022, "Effect of springing and whipping on exceedance probability of vertical bending moment of a ship," Ocean Engineering, **266**, p. 112600.

[3] Gan, J., Liu, X., Wang, Z., and Wu, W., 2021, "Experimental study on the fatigue damage of designed T-type specimen with high-low frequency superimposed loading," International Journal of Fatigue, **143**, p. 105985.

[4] Gan, J., Liu, X., Liu, H., Wang, Z., and Wu, W., 2022, "Effect of high-low frequency superimposed loading on the fatigue crack propagation of longi-web connection joint," International Journal of Fatigue, **163**, p. 107043.

[5] Gaspar, B., Teixeira, A., and Guedes Soares, C., 2016, "Effect of the nonlinear vertical wave-induced bending moments on the ship hull girder reliability," Ocean Engineering, **119**, pp. 193–207.

[6] Storhaug, G., 2007, "Experimental investigation of wave induced vibrations and their effect on the fatigue loading of ships," (Doctoral dissertation) Norwegian University of Science and Technology (NTNU), Oslo.

[7] Lloyd's Register, 2023, *Guidance Notes for General Overview of Ship Structural Vibration Problems*, Lloyd's Register Group Limited, International Maritime Organization, International Labour Organization or Maritime and Coastguard Agency.

[8] Lotsberg, I., 2016, *Fatigue design of marine structures*, Cambridge University Press, New York NY.

[9] Naess, A. and Moan, T., 2012, *Stochastic Dynamics of Marine Structures*, Vol. 9780521881555, Cambridge University Press, New York.

[10] Bouscasse, B., Merrien, A., Horel, B., and De Hauteclocque, G., 2022, "Experimental analysis of wave-induced vertical bending moment in steep regular waves," Journal of Fluids and Structures, **111**, p. 103547.

[11] Waskito, K. T., Kashiwagi, M., Iwashita, H., and Hinatsu, M., 2020, "Prediction of nonlinear vertical bending moment using measured pressure distribution on ship hull," Applied Ocean Research, **101**, p. 102261.

[12] Zhao, W., Leira, B. J., Feng, G., Gao, C., and Cui, T., 2021, "A reliability approach to fatigue crack propagation analysis of ship structures in polar regions," Marine Structures, **80**, p. 103075.

[13] Fang, X., Liu, G., Wang, H., Xie, Y., Tian, X., Leng, D., Mu, W., Ma, P., and Li, G., 2022, "Fatigue crack growth prediction method based on machine learning model correction," Ocean Engineering, **266**, p. 112996.

[14] Lee, D. and Kwon, K., 2023, "Dynamic Bayesian network model for comprehensive risk analysis of fatigue-critical structural details," Reliability Engineering System Safety, **229**, p. 108834.

[15] DNV (Det Norske Veritas), 2021, *Finite element analysis*, (DNVGL-CG-0127).

[16] ANSYS, 2023, *Workbench User's Guide*, Ansys Inc, Canonsburg, PA, USA, https://ansyshelp.ansys.com/account/secured?returnurl=/Views/Secured/corp/v232/en/wb2_help/wb2_help.html%23wb2_help

[17] DNV (Det Norske Veritas), 2021, *Fatigue design of offshore steel structure*, (DNVGL-RP-C203).

[18] Adland, R., Cariou, P., and Wolff, F.-C., 2020, "Optimal ship speed and the cubic law revisited: Empirical evidence from an oil tanker fleet," Transportation Research Part E: Logistics and Transportation Review, **140**, p. 101972.

[19] Lakshmynarayanana, P. A. and Hudson, D., 2017, "Estimating Added Power in Waves for Ships Through Analysis of Operational Data," 2nd Hull Performance and Insight Conference, Germany.

[20] Soares, C. and Moan, T., 1991, "Model uncertainty in the long-term distribution of wave-induced bending moments for fatigue design of ship structures," Marine Structures, **4**(4), pp. 295–315.

[21] IACS (Det Norske Veritas), 2012, *Common structural rules for double hull oil tankers*, International Association of Classification Societies, London.

[22] Melchers, R. E., 1999, "Structural reliability : analysis and prediction," .

[23] Yong, B. and Wei-Liang, J., 2016, *Marine Structural Design (2nd Edition)*, Elsevier.

[24] Breitung, K., 1984, "Asymptotic Approximations for Multinormal Integrals," Journal of Engineering Mechanics, **110**(3), pp. 357–366.

[25] Hohenbichler, M. and Rackwitz, R., 1981, "Non-Normal Dependent Vectors in Structural Safety," Journal of the Engineering Mechanics Division, **107**(6), pp. 1227–1238.

[26] Rosenblatt, M., 1952, "Remarks on a Multivariate Transformation," The Annals of mathematical statistics, **23**(3), pp. 470–472.

[27] DNV, 2004, *SESAM USER MANUAL Proban Theory*, Det Norske Veritas, Høvik.

[28] DNV, 2004, *SESAM USER MANUAL Proban*, Det Norske Veritas, Høvik.

[29] Almar-Næss, A., 1985, "Fatigue handbook : offshore steel structures," .

[30] Gao, J. and Yuan, Y., 2020, "Probabilistic model of fatigue damage accumulation of materials based on the principle of failure probability equivalence," Structures, **28**, pp. 659–667.

[31] Newman, J. and Raju, I., 1981, "An empirical stress-intensity factor equation for the surface crack," Engineering Fracture Mechanics, **15**(1), pp. 185–192.

[32] British Standard, 2005, *Guide to methods for assessing the acceptability of flaws in metallic structures*, (BS7910:2005).

[33] ABS, 2020, *Guide for fatigue assessment of offshore structures*, American Bureau of Shipping, Texas, USA.

List of Figures

List of Tables